FORMATION OF MULTIPLE MICRO-VORTICES IN REGIONS OF ION CONCENTRATION POLARIZATION

by

SRINIVAS KUMAR GOWRANGA HANASOGE

A thesis submitted to the

Graduate School-New Brunswick

Rutgers, The State University of New Jersey

In partial fulfillment of the requirements

For the degree of

Master of Science

Graduate Program in Mechanical and Aerospace Engineering

Written under the direction of

Dr. Francisco J. Diez

And approved by

_____

_____

_____

New Brunswick, New Jersey

MAY 2014

ABSTRACT OF THE THESIS

Formation of multiple micro-vortices in regions of ion concentration polarization

by SRINIVAS KUMAR GOWRANGA HANASOGE

Thesis Director:

Dr. Francisco J. Diez

Ion transport in nano-scale channels is of interest due to their perm-selective behavior, occurring due to the overlap of electric double layers. This leads to a variety of interesting electrokinetic phenomenon in regions around the nano-pores including, ion concentration polarization, field amplified sample stacking and formation of micro vortex instability among others. Incorporating nano-pores within microfluidic systems in functional lab-on-a-chip devices has resulted in techniques for better sample handling, fluid manipulation, and mixing. Effects of concentration polarization on local hydrodynamics was studied experimentally near a nano-porous membrane incorporated in a Micro-channel in this thesis. Along with the formation of depletion and pre-concentration regions in the setup, we observe additional effects of field amplification on local hydrodynamics. We report the direct observation of a primary micro-vortex instability in the depletion region of ICP, along a plane perpendicular to the substrate. This hydrodynamic effect is directly attributed to the non-uniform electro osmotic slip along the micro channel's bottom wall due to field amplification. In addition to the primary vortex, we also

note the formation of a secondary, tertiary and subsequent vortices along the length of the depletion region. A physical model is proposed which considers the two dimensionally varying concentration profile in the depletion region to account for the formation of multiple vortices. The mixing effect of the fast moving primary vortex in a two dimensionally varying concentration profile changes the local concentration in the depletion region. This in turn affects electro-osmotic slip velocity, leading to the formation of multiple vortices. We perform numerical analysis on simpler, slipping wall models, which show excellent agreement with the experimental results.

Acknowledgements

I would like to firstly thank my advisor Dr. Javier Diez for all his support and encouragement towards my thesis. He is a great mentor and always encouraged me to push my limits a little more. I thank him for giving me the wonderful opportunity to work on this project, And especially for his moral support during difficult times which I will always remember.

A sincere thanks to Dr. German Drazer for being a great mentor and also supporting me through my research work. It was a privilege collaborating with his group and a great learning opportunity. Thanks to Dr. Shahab Shojaei Zadeh for being a part of the committee and reviewing my thesis. Special thanks to Dr. Raghavendra whose technical guidance I value and all the moral lectures that helped me through my course.

No acknowledgement would be complete without thanking my family and friends, especially my lab mates, Arturo, Mena and Tom. All of them have helped me tremendously to complete my work. My brother, for his love and support throughout my stay away from home. I thank my parents for their faith in me and allowing me to be as ambitious as I wanted. And Niveditha for being the pillar of support throughout my Engineering career.

Dedication*:*

Dedicated to my Grandfather,

Late Shri Krishnamurthy Hanasoge Narayanarao

Without whose support my work would not have been possible.

ಪ್ರೀತಿಯ ಅಜ್ಜನಿಗೆ ಅರ್ಪಣೆ

ನಿಮ್ಮ ಜೀವನವೇ ನನಗೆ ಸ್ಫೂರ್ತಿ

Contents

ABSTRACT OF THE THESIS ii
Acknowledgements iv
Dedication v
List of Figures: vii
1. Introduction: 1
1.1 Electric Double Layer: 2
1.2 Electrokinetic phenomenon and electro-osmosis: 3
1.3 Electrokinetic effect in nano-scale: 4
1.4 Ion Concentration Polarization: 5
1.5 Current voltage characteristics of an ideal ion-selective membrane: 6
1.6 ElectroKinetics of the second kind: 6
1.7 Induced charge Electro-osmosis (ICEO): 7
1.8 Micro Vortices: 8
1.9 Concentration, Electric Potential and Electric field strength in the depletion region: 9
2. Methods and Materials: 20
2.1 Micro fabrication and soft lithography 20
2.2 Micro fluidic device: 21
3. Results and Discussion: 26
3.1 Field Amplified Sample Stacking (FASS) 26
3.2 Generation of Micro-Vortices: 28
3.3 Discussion on the observed vortices: 29
3.3.1 Multiple Vortices: 31
4. Simulation: 42
4.1 Vortex Identification: 43
5. Conclusion: 49
References 51

List of Figures:

Figure 1: Schematic of the formation of Electric double layer at a solid-liquid interface. (a) Shows the redistribution of ions near the interface. (b) Shows the electro potential as function of distance from the surface. (c) Shows the concentration of co-ions and counter ions as a function of distance from the interface. 11

Figure 2: Electro-osmotic flow in a micro-channel. (a) Shows the thin double layer case in a micro channel (i.e. the width of double layer is small compared to the characteristic dimension of micro channel). (b) Comparison of velocity profile in open channel and closed micro-channel. 12

Figure 3: Comparison between the cases of thin, and overlapping double layers. (a) Shows the thin double layer case in a micro channel. (b) Shows cases for overlapping double layer (Nano channel). 13

Figure 4: The concentrations of ions on the anodic and cathodic regions of the membrane are shown. Curve 1 represents the ohmic regime, in which the diffusion flux compensate for the removal of anions on the right side of the membrane. Curve 2 shows the over-limiting regime in which an extended space charge is formed. 14

Figure 5: Graph shows the behavior of current in the ohmic, limiting and over-limiting regimes of voltage. ((Rubinstein et al., 2008)) 15

Figure 6: Formation of vortices due to electrokinetics of the second kind near a flat membrane. 16

Figure 7: Corner in a micro channel which gets polarized due to finite permittivity of the channel wall material. The arrows show the direction of electro-osmotic flow which will result in an ejecting flow 17

Figure 8: Comparison between the 3 different kinds of vortices. (a) Shows corner cortex due to ICEO flow. ((Thamida & Chang, 2002)). (b) Shows vortices induced due to electro-osmosis of the second kind. ((Rubinstein et al., 2008)) (c) Vortices due to non-uniform electroosmotic slip at the micro channel walls. ((Yossifon & Chang, 2010)) 18

Figure 9: Variation of concentration, electric potential and electric field as function of distance from the membrane for a 1D model. (a) Shows the linear concentration profile in the depletion region. (b) Shows the non-dimensional electric potential in the depletion region. (c) Non-dimensional Electric field strength in the region of depletion. 19

Figure 10: Flow chart of the Photo lithography process used for micro-fabrication process. The second image shows the soft-lithography used to make replicas of the master. 23

Figure 11: Schematic of the experimental setup, showing the fluorescence microscopy setup. . 24

Figure 12: Schematic of the experimental setup. (a) Shows top view of the experiment. (b) Shows the side view. Note that, nafion is present only on the bottom wall. This is clear from (b). 25

Figure 13: (a) Working of Field Amplified sample stacking (REF). For t>0 after the electric field is applied, it is observed how the negative ions stack at the entrance of the depletion region. (b) Shows the velocity profile in the region of low electrolyte concentration, and bulk 33

Figure 14: Field Amplified sample stacking. Shows the stacking phenomenon at different times. The shape of the stacking front is also clear. From Kim et al, 2012. 34

Figure 15: Experimental observation of the vortices formed due to non-uniform slip in the depletion region..... 35

Figure 16: Side view of the vortex. The tear-drop shape of the vortex is evident. See supplementary video. 36

Figure 17: Initial shape of vortex before back pressure builds up in the system. 37

Figure 18: Summarizing the phenomenon of non-linear electro-osmotic slip. (a) Shows the linear dip in concentration. (b) The electric potential along the channel. (c) Electro-osmotic slip velocity and (d) the formation of micro vortices. 38

Figure 19: (a) Showing the side view of the three vortices formed in the depletion region. (b) Showing the direction of the three vortices, (c) Trajectory of a single particle that goes around all three vortices. 39

Figure 20: Schematic of the concentration variation in 2D from the side view, and the mixing effect of vortices changing local concentration..... 40

Figure 21: Schematic, showing the formation of multiple vortices. (a) Concentration change in the depletion region near bottom wall. (b)Electric potential in the depletion region. (c) Electro-

osmotic slip along the channel's bottom wall. (d) Side view, showing the formation of multiple vortices. Due to enhanced mixing, local region of higher concentration lead to the formation of multiple vortices. 41

Figure 22: Geometry used for the numerical analysis, along with the applied boundary conditions. Mesh used for the simulation is also shown. 45

Figure 23: (a) Stream lines from non-uniform acceleration boundary condition. (b) Velocity magnitude 46

Figure 24: Shows the results from simulation, the effect of mixing and formation of secondary, and tertiary vortex. (a) Streamlines (b) Velocity magnitude. 47

Figure 25: Detection of vortex by delta method. (a) Shows the overlap of streamlines and predictions by delta method for the velocity profile assumed in this case. (b) Overlap of streamlines and predictions by delta method for the velocity profile as predicted by kim et al, 2012. 48

1. Introduction:

Study of fluid transport at micro and nano scales has gained much importance in the last decade primarily due to the rapid development of micro and nano the fabrication techniques. Microfluidic devices allow the use of small quantities and very small volumes of sample, which are an advantage and enable the working of smaller and portable lab-on-chip devices. For handling very small volumes of fluid, a microfluidic device makes use of many components such as valves, pumps, sensors, mixers, filters, separators, heaters etc.

Fluid handling at micro scale is usually induced by pressure, electric field, magnetic field, gravity, or capillary forces. Electrokinetics refers to the coupling between electric currents and mass flow in electrolytes. In general, as the surface to volume ratio of the channel increases, the use of electric field in pumping the flow becomes important. The electrokinetically driven flow depends linearly on the applied electric field, and is not affected much by the channel size. This make it the more attractive option for fluid transfer in micro-nano scales.

The dynamics of charge transport, however, change inside a nano channel. As the surface to volume ratio is high in nano channels, the transport is governed by surface charge. This leads to nano-channels showing ion selective permeability, allowing the passage of only one kind of ions. This perm selective behavior of nano-channels gives rise to many interesting phenomenon like, ion concentration polarization, field amplified sample stacking, generation of micro vortices, formation of a secondary space charge etc. Understanding these phenomena is important in micro fluid handling, mixing and separation techniques. By incorporating nano-channels within microfluidic systems, functional lab-on-a-chip devices have been created for sample preparation, separation, and detection.

This thesis starts with a review of the basic concepts of electrokinetics in chapter 1. First, the formation of electric double layer is discussed, and then the basic electrokinetic phenomenon, electro-osmosis is reviewed. The effect of channel geometry, and the consequence of overlap of double layer in nano-scales is discussed in section 1.3. Ion- concentration polarization and the current voltage characteristics of an ideal nano-porous membrane is discussed in sections 1.4, 1.5. A brief review of electrokinetics of the second kind and induced charge electro-osmosis (ICEO) is discussed in section 1.6, 1.7 respectively. Experimental methods and materials used are presented in Chapter 2. The various steps in the fabrication process, and the experimental setup are discussed. Most of the observations made are visual, and are discussed in Chapter 3. 2-Dimensional hydrodynamic simulation of the model problem is presented in chapter 4. Conclusion and scope for future work is discussed in Chapter 5.

1.1 Electric Double Layer:

In an electric double layer there is a polarization of charged species at the interface between a fluid and an immersed body. The electric double layer is the fundamental phenomenon that gives rise to all the electrokinetic effects, and for this study, consider the double layer formed at the interface between a solid and liquid. The ions are adsorbed onto the solid due to chemical interactions, dissociation or ionization of surface groups, among others (Zhao & Yang, (2012)). This leads to two parallel layers of charge surrounding the solid. The first layer comprises of ions (co-ions) adsorbed into the solid leading to a net surface charge. The second layer consists of ions (counter ions) attracted to this surface charge due to coulombs force, which electrically screens the first layer. Co-ions and counter ions are the ions that have the same kind of charge as the first and second layer respectively. For example, if a wall has net negative surface charge,

the positive ions in the electrolyte surrounding it are the counter-ions, and negative ions are the co-ions.

The second layer of counter-ions consists of many regions as shown in Figure 1. This simple model of the electric double layer is suggested by Otto Stern. This model predicts the existence of an inner stern layer, and an outer diffuse layer of charge in the second layer. The inner stern layer is strongly bound to the wall surface and is immobile. The outer diffuse layer is loosely bound to the wall and can be moved by applying an electric field tangential to it. The stern layer and diffuse layer are separated by a stern plane. The electric potential changes little within the stern layer and decreases to zero in the diffuse layer. The mobile inner part of the electric double layer is located between one to two radii away from the surface, and this boundary is known as the shear plane. It is on this plane where the no-slip fluid flow boundary condition is assumed to apply. The potential at the shear plane is referred to as the zeta potential (ζ) (Masliyah and Bhattacharjee (2006)), the thickness of the double layer is called the Debye length and scales to a few nano-meters. The interaction between the diffuse part of the double layer and an electric field applied externally is called the Electrokinetic phenomenon.

(Most experimental studies report cations as the counter ions in their experiment. The same will be considered for all discussions henceforth)

1.2 Electrokinetic phenomenon and electro-osmosis:

The diffuse layer in the double layer is loosely bound to the wall surface and can interact with externally applied electric field. This interaction of the mobile ions causes their movement along the direction of field applied leading to a slipping plane of charge. This slipping layer of charge, due to viscous stresses moves the fluid bulk far from the surface. The bulk motion of the electrolyte past a fixed surface in the presence of an electric field is called electro-osmosis.

The slipping velocity is called smoluchowski slip velocity, where

$$u = -\frac{\varepsilon \psi E}{\mu}$$

Figure 2a shows the electro-osmotic flow profile in an open micro channel (width of micro channel is larger than thickness of the double layer.) The walls of the channel induce a diffuse layer of counter ions, these get attracted to the electrode of opposite polarity and move the fluid bulk due to viscous effects. This leads to an overall uniform plug like flow in the micro channel. The plug flow has a velocity equal to the smoluchowski slip velocity, and is therefore directly dependent on the applied electric field. Due to the plug profile of the flow, there are no diffusion non-uniformities. Figure 2b shows the comparison between the velocity profiles in an open and closed micro-channel. For a closed micro-channel, the fluid flow along the slip direction leads to a backpressure flow, to maintain conservation of mass. This backpressure flow has a parabolic profile as seen in the Figure 2b.

1.3 Electrokinetic effect in nano-scale:

When the size of the channel is decreased to a few nano-meters, the surface to volume ratio is very large. This results in a surface charge driven flow inside the channel. At nanometer scale, the channel dimensions are comparable to the thickness of the double layer. Therefore, if the channel width is small enough, the double layers from opposite walls overlap, resulting in a net counter-ion charge inside the nano-channel and expelling any co-ions. Figure 3 shows the comparison between non-overlapping and overlapping double layers from opposite walls. Since the width of the double layer is dependent on the concentration of ions, a low concentration electrolyte produces a thicker double layer. This results in an overlap of double layers at these length scales. The phenomena encountered in nanofluidic devices are appreciably different from

those in microfluidics due to this overlap of double layers. The presence of only counter ions in the nano-channel leads to ion-selective behavior of the channel. The nano-channel with overlapping double layer will therefore be permeable only to counter ions, preventing any passage of co-ions.

1.4 Ion Concentration Polarization:

Ion concentration polarization (ICP) is the redistribution of ions into regions of low concentration (depletion) and high concentration (enrichment) across a nano-channel. This primarily occurs due to the perm selective nature of the nano-channel. In most experimental studies (Kim, Li, and Han (2009); Lee, Song, and Han (2008); Yossifon and Chang (2010)), the nano-slots have cations as the counter-ions. This leads to a case where both the anions and cations are enriched on the cathodic side of the nano-slot, and both are depleted on the anodic side.

To understand how ICP works, let us assume an ideally perm-selective nano porous membrane or even a single nano channel with positive ions as the counter ions. At low voltage conditions, the electrolyte concentration decreases on the side of the membrane where the counter ions enter from the electrolyte (anodic side). This happens because, the co-ions move away from the membrane towards the electrode leading to a decrease in the co-ion concentration as this decrease is not compensated by their intake from the membrane. To maintain electro neutrality there is a diffusion flux acting from electrolyte towards the membrane on the counter ions (Figure 4). Thus the diffusion layer is formed. Overall, depletion of both counter and co ions occurs at the anodic side. The concentration decrease in the depletion region is linear for a 1D model (Yossifon et al. (2010)). Refer Figure 4 curve 1 for concentrations in the device. The

highest concentration drop is C_o, and this corresponds to the maximum diffusion flux in the depletion region.

On the cathodic side of the membrane, there is an accumulation of co-ions as they are not allowed to migrate into the membrane. This leads to an increase in the concentration of anions, and therefore cations to maintain electro neutral condition.

1.5 Current voltage characteristics of an ideal ion-selective membrane:

Consider the case in which the ions can move across a membrane by only passing through it. This means that the membrane prevents an overall electro-osmotic flow towards the cathode. In such a case, when a low voltage is applied across the reservoirs, the current changes linearly with the voltage (ohmic region.) However, the formation of depletion region acts as a resistance to the circuit, therefore limiting the current in the circuit at higher voltages. This is called the limiting current regime. Theoretically, the current in the circuit should drop further at higher voltages. However, experimentally, a further increase in voltage results in further increase of current beyond the limiting regime. This region is called the over-limiting current regime. Figure 5 shows the typical current-voltage behavior of such a system. This increase in current in the over limiting regime is attributed to the formation of an extended space charge, and vortices in the depletion region. The formation of this extended space charge leads to electrokinetics of the second kind (first reported by Dukhin s.s, 1991). This phenomenon will be reviewed in the following section.

1.6 ElectroKinetics of the second kind:

When the voltage in the system is increased beyond the limiting regime, a further decrease in the concentration of the electrolyte is not possible, therefore the removal of anions in the

depletion region is not compensated by the diffusion flux of cations towards the membrane. This leads to an overall net positive charge next to the membrane surface. A deviation from electro-neutrality in this region is noted. This is shown by curve 2 in Figure 4. This excess charge is called the induced space charge as it is not directly connected to the membrane surface. This induced space charge causes electrokinetics of the second kind.

The extended charge layer has a length scale comparable to that of Debye length. This extended charge layer, however, is induced by the normal component of the applied electric field and exists as long as the external field exists. Researchers have argued that due to local disturbances in the system, the electric field strength gets amplified (Rubinstein et al. (2008). This causes a high pressure spot, leading to a radial outflow of fluid, causing the formation of a vortex pair. Researchers have experimentally shown how electrokinetics of the second kind leads to a hydrodynamic vortex instability (Rubinstein et al. (2008)). It is also important to note that the vorticity in this case is in a direction perpendicular to the chip substrates. See Figure 6 for a schematic for the formation of such vortices.

1.7 Induced charge Electro-osmosis (ICEO):

Formation of hydrodynamic instability is noted in several other cases. One such case in which non-uniform surface charge induces a pair of vortex instability is ICEO. When there is a polarizable material (or across a corner in a micro-channel) under the influence of an electric field, the material is polarized, with different regions of the material having different surface charge. Let us consider the cases of electric field across a corner (Figure 7). It is clear how the positive charge is accumulated on one side and negative charge on the other. This occurs due to the finite permittivity of the material. As a consequence of this, the zeta potential of the material changes near the two oppositely charged surfaces (i.e. positive ions accumulate near

the negative surface, and vice versa). Further, the tangential component of the applied electric field leads to an opposing slip velocity due to opposite charges. This results in an ejecting flow in the system, which can be a vortex in some cases. The principle of ICEO flow is explained in Figure 7.

1.8 Micro Vortices:

Micro vortices are reported by many authors in micro-fluidic devices. Researchers have tried using vortices in micro fluidic devices for mixing fluids, particle separation, nano-colloid detection etc. It is therefore essential to conduct a detailed study on the formation of vortices in microfluidic devices. Researchers have observed vortices in micro fluidic devices in many cases. They are mainly classified into three different kinds.

1. *Induced charge corner vortex*: These are usually seen at the corners of a micro channel or near a conductive species in a micro channel. They occur due to the finite polarizability of the channel material, giving rise to polarization of channel walls with opposite charge. This further leads to electro-osmotic slip velocity in opposing directions, leading to an ejecting flow. Ejecting flow further leads to a vortex. This kind of vortex occurs at all ionic concentrations (Thamida & Chang, (2002)). Researchers have observed these vortices around conductive spheres as well (Squires and Bazant (2004)).
2. *Vortices arising due to an extended polarized layer of charge:* This occurs due the electrokinetics of the second kind, and formation of a secondary space charge layer (Dukhin, (1991)). These vortices are seen only at low ionic strengths and in the over limiting regime in the depletion region of ICP. The direction of vorticity is perpendicular to the chip substrates (Rubinstein et al. (2008)).

3. *Vortices due to the non-linear electro-osmotic slip*: These are vortices that form as a result of non-uniform slip velocity along the walls of the micro channel. In regions of depletion, the electric field is amplified and hence the slip velocity is higher, leading to a vortex flow to maintain mass continuity. The direction of vorticity is parallel to the chip substrates.

The above stated three kinds of vortices are experimentally reported in the literature. Figure 8 shows a comparison of the three.

Many researchers have performed detailed analysis on the first and second kind of vortices mentioned above. In this study an analysis of the vortex induced due to non-uniform electro-osmotic slip velocity is presented. These vortices are observed while performing experiments on ion concentration polarization.

1.9 Concentration, Electric Potential and Electric field strength in the depletion region:

The concentration decrease for a 1D model is shown in Figure 9. This formulation has been suggested by researchers (Yossifon et al. (2010)) to work well for a nano-porous membrane. The electric potential and electric field strengths in the depletion region can be calculated using this method. From Yossifon et al. (2010) the concentration and electric potential are calculated according to these formulae.

$$\tilde{C} = 1 - \tilde{x}$$

$$\tilde{\phi} = \frac{1}{z_-} \ln(1 - \tilde{x})$$

Here $\tilde{C}$ is the non-dimensional concentration, $\tilde{\phi}$ is the non-dimensional electric potential.

The electric field strength is calculated from the potential ($\tilde{\phi}$). Figure 9c shows the non-dimensional electric field for a 1D nano-porous membrane.

This concludes the introduction to the thesis. The experimental setup and the details of the techniques used are discussed in the next chapter.

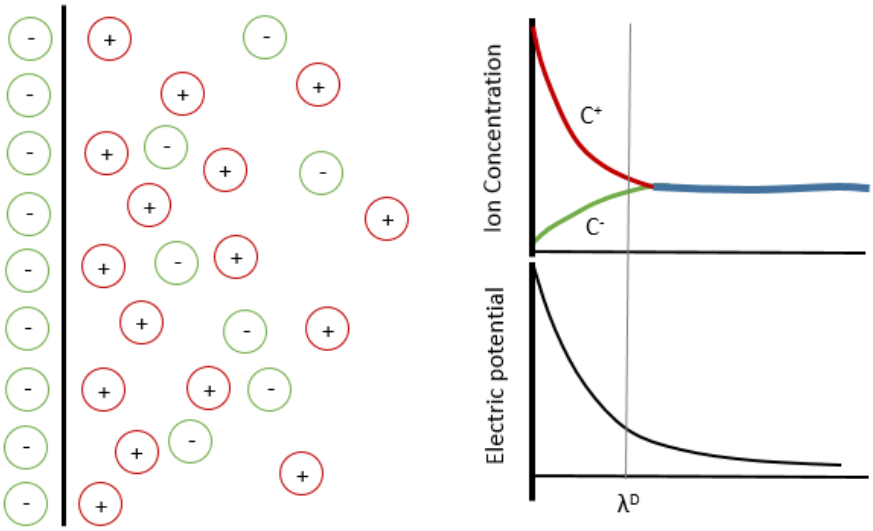

Figure 1: Schematic of the formation of Electric double layer at a solid-liquid interface. (a) Shows the redistribution of ions near the interface. (b) Shows the electro potential as function of distance from the surface. (c) Shows the concentration of co-ions and counter ions as a function of distance from the interface.

(a)

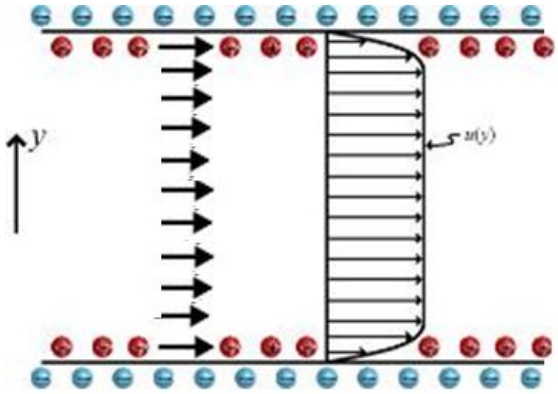

(b)

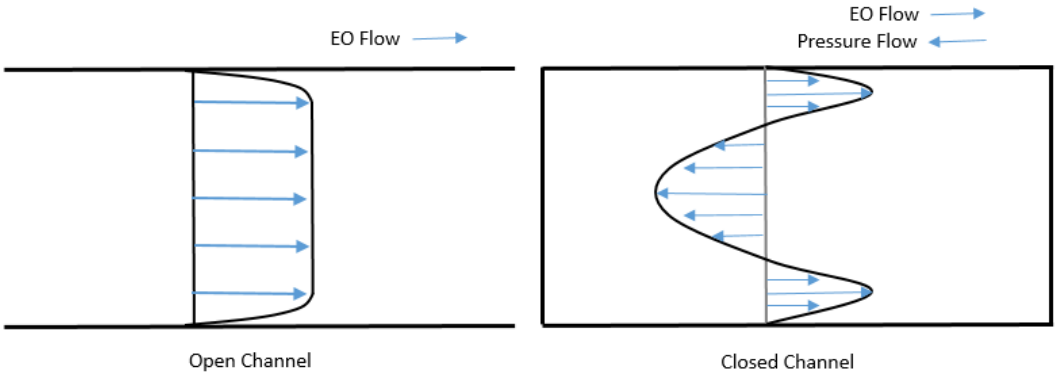

Figure 2: Electro-osmotic flow in a micro-channel. (a) Shows the thin double layer case in a micro channel (i.e. the width of double layer is small compared to the characteristic dimension of micro channel). (b) Comparison of velocity profile in open channel and closed micro-channel.

(a)

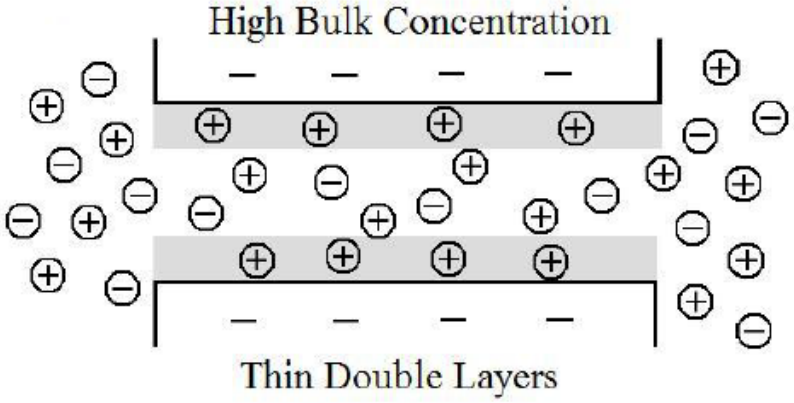

(b)

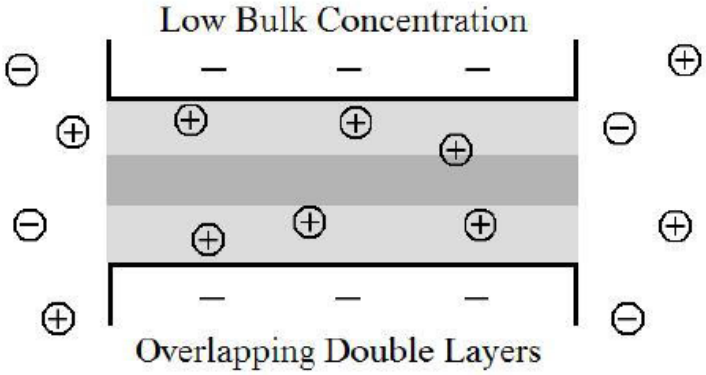

Figure 3: Comparison between the cases of thin, and overlapping double layers. (a) Shows the thin double layer case in a micro channel. (b) Shows cases for overlapping double layer (Nano channel).

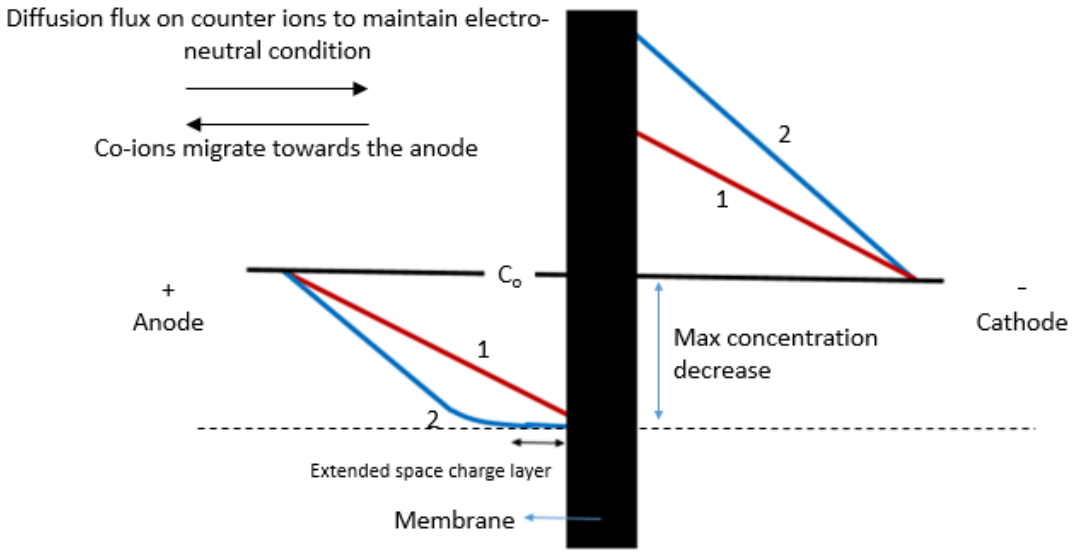

Figure 4: The concentrations of ions on the anodic and cathodic regions of the membrane are shown. Curve 1 represents the ohmic regime, in which the diffusion flux compensate for the removal of anions on the right side of the membrane. Curve 2 shows the over-limiting regime in which an extended space charge is formed.

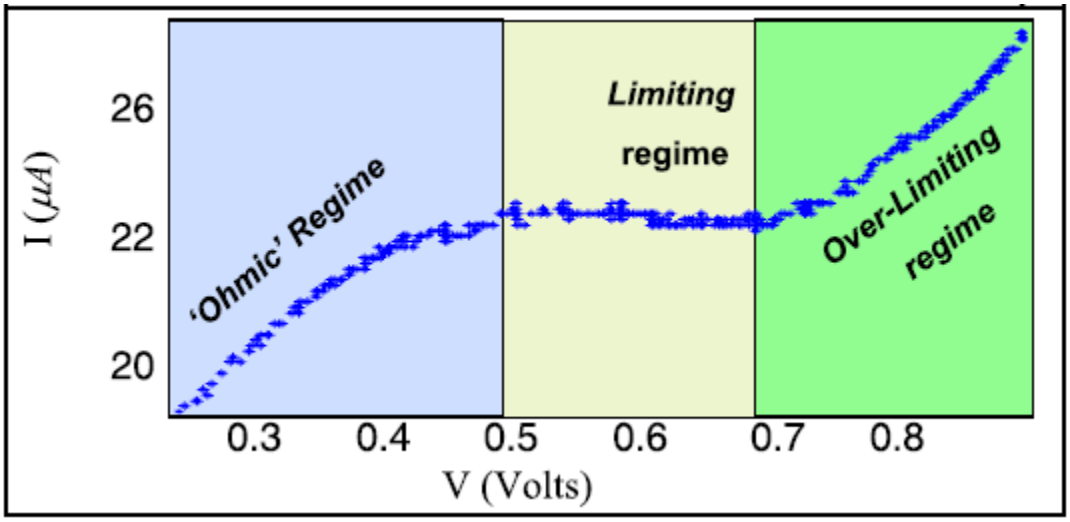

Figure 5: Graph shows the behavior of current in the ohmic, limiting and over-limiting regimes of voltage. ((Rubinstein et al., 2008))

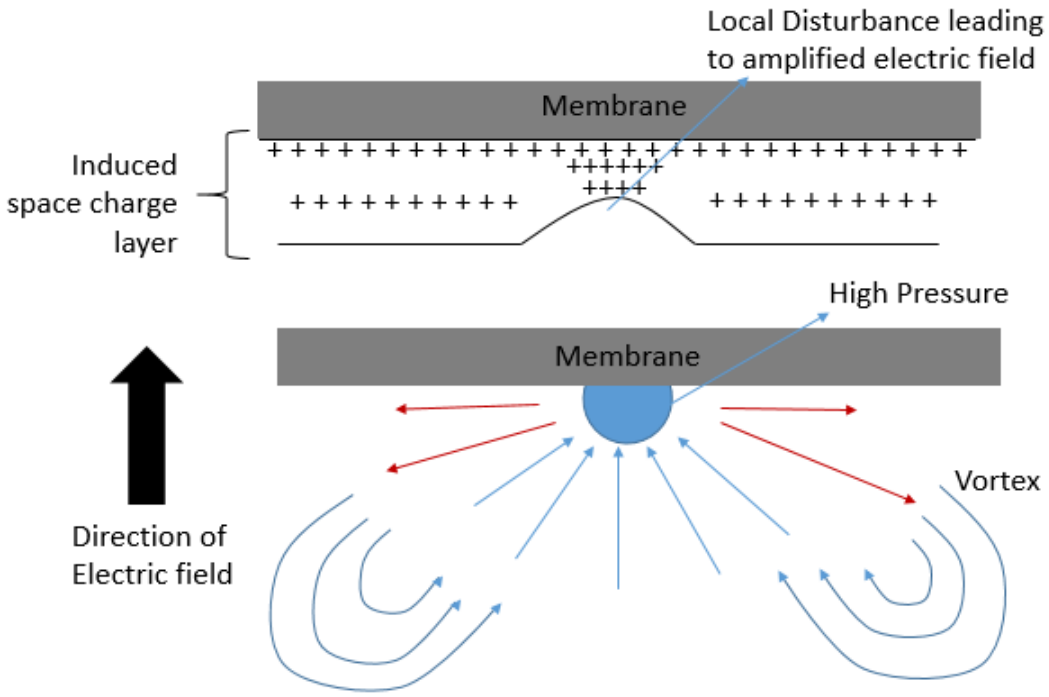

Figure 6: Formation of vortices due to electrokinetics of the second kind near a flat membrane.

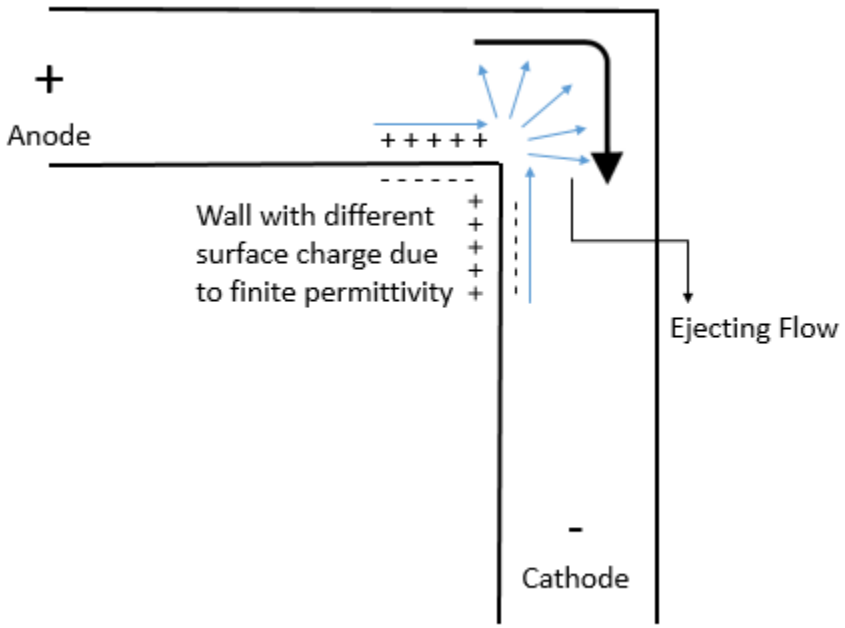

Figure 7: Corner in a micro channel which gets polarized due to finite permittivity of the channel wall material. The arrows show the direction of electro-osmotic flow which will result in an ejecting flow.

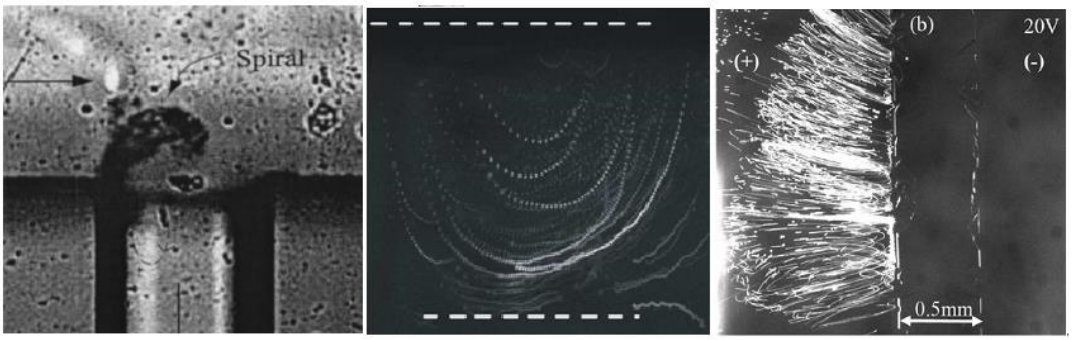

Figure 8: Comparison between the 3 different kinds of vortices. (a) Shows corner cortex due to ICEO flow. (Thamida & Chang, (2002)). (b) Shows vortices induced due to electro-osmosis of the second kind. (Rubinstein et al. (2008)) (c) Vortices due to non-uniform electroosmotic slip at the micro channel walls. (Yossifon and Chang (2010))

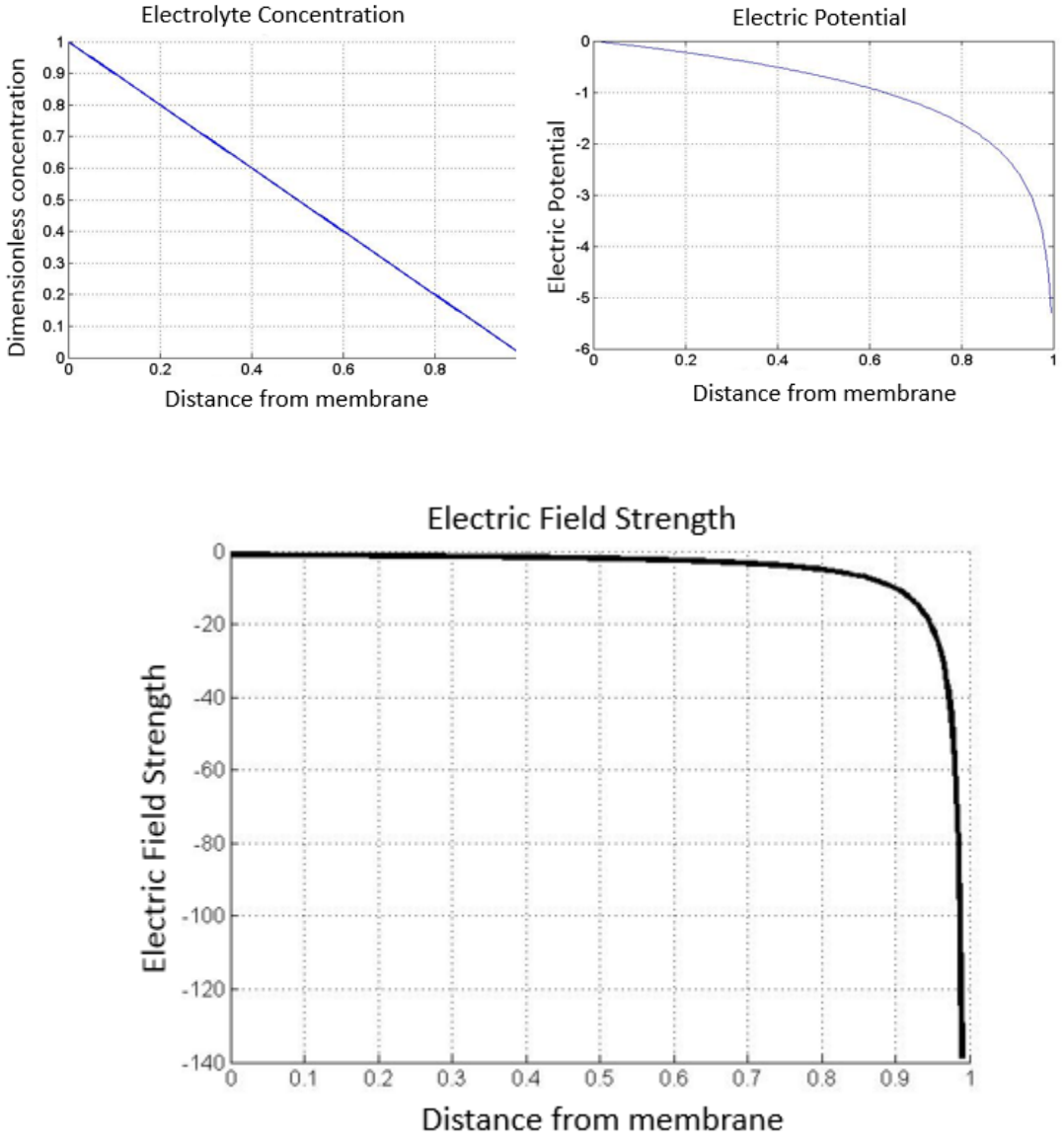

Figure 9: Variation of concentration, electric potential and electric field as function of distance from the membrane for a 1D model. (a) Shows the linear concentration profile in the depletion region. (b) Shows the non-dimensional electric potential in the depletion region. (c) Non-dimensional Electric field strength in the region of depletion.

2. Methods and Materials:

2.1 Micro fabrication and soft lithography:

Standard lithography techniques, such as photolithography and soft-lithography, are used to fabricate devices. First, photoresist is coated on a silicon wafer or a glass substrate. A spin coater (Laurell Technologies Inc.) is used to coat a uniform thin layer of photoresist film on either substrate. After the resist is soft baked and cooled, it's exposed to UV light in a mask aligner through a photomask on which the image of the device is drawn. A two dimensional latent image is formed on the resist. When the UV light is passed through a mask, the opaque pattern blocks the light and the clear regions allow the light beam to pass through, thus enabling a transfer of pattern on photoresist. It is later developed in a developer solution to form a 3 dimensional master mold of the image. Figure 10 shows the flow chart of the micro-fabrication procedure used.

Channels are made using poly (dimethylsiloxane) (PDMS) by the standard process of soft lithography (Figure 10). This is done by mixing 10 to 1 ratio of the elastomer and hardener and curing at 80 degrees for 3 hours. These PDMS replicas are then peeled off from the silicon substrate and bonded to a glass slide. This bonding is done by first treating the surface of PDMS and glass in an oxygen plasma for 1 minute, and then pressing them together to bond permanently. Reservoirs are dug into the PDMS micro channels before they are bonded to the glass slide, using a mechanical punch.

Cured nafion is used as the nano porous membrane in these experiments. Nafion is a sulfonated tetrafluoroethylene based fluoropolymer-copolymer, and acts as a cation selective membrane when cured. In the experiments, nafion 117 in solution form is used to pattern the

membrane on a glass slide. This is done by passing the nafion through a temporarily bonded PDMS micro channel on the glass slide. Once the nafion completely wets the surface, the temporarily bonded PDMS micro channel is removed and cured at 80 degrees for 10 minutes. A PDMS micro channel is then irreversibly bonded using an oxygen plasma on the glass slide containing the patterned nafion. Nafion molecules have a ring like structure which results in them behaving as nano-pores. The size of these nano-pores scale to 5nm. Similar methodology for the fabrication of nano-pores is followed by (Lee, Song, and Han 2008).

Fluospheres (Invitrogen) with 1um diameter are used to track the flow in the micro-channel. Fluorescent b-phycoerythrin (Anaspec) dye is used to study the enrichment and depletion regions. This dye is negatively charged and hence behaves as co-ions in these experiments (Dark regions indicate a depletion region, and bright regions indicate enrichment of negative ions). The fluospheres and dye chosen have similar fluorescent properties, i.e. they absorb and emit in the same regions of spectrum, therefore enabling us to visualize them simultaneously.

A Nikon Ti inverted microscope, equipped with an X-cite mercury light source is used in the experimental setup. Absorption and emission filter with range from 540-552nm and 565-607nm respectively are used. A Rolera Mgi video camera is used to capture the images and video. Figure 11 shows a schematic of the experimental setup.

2.2 Micro fluidic device:

The schematic of the micro fluidic device is shown Figure 12. Nafion is surface patterned on a glass slide, and a PDMS micro channel is bonded on the cured nafion. Since the cured nafion is only at the bottom wall of the micro channel, an overall electro-osmotic flow in the channel is expected. This happens due to the space above the membrane which allows the flow of bulk fluid. Figure 12b shows the side view of the channel, and it shows how the fluid bulk can flow in

system. Particles and dye are introduced in a 0.1mM buffer solution from the reservoirs. Care is taken to ensure that the channel walls are completely wet before any voltage is applied, to ensure that there are no bubbles in the channel that will block the flow and electric field. A voltage is applied across the reservoirs using standard platinum electrodes. The flow of particle and dye in the channel are simultaneously recorded using the video camera.

A number of variations of this setup are used in different experiments. These will be discussed in the results section.

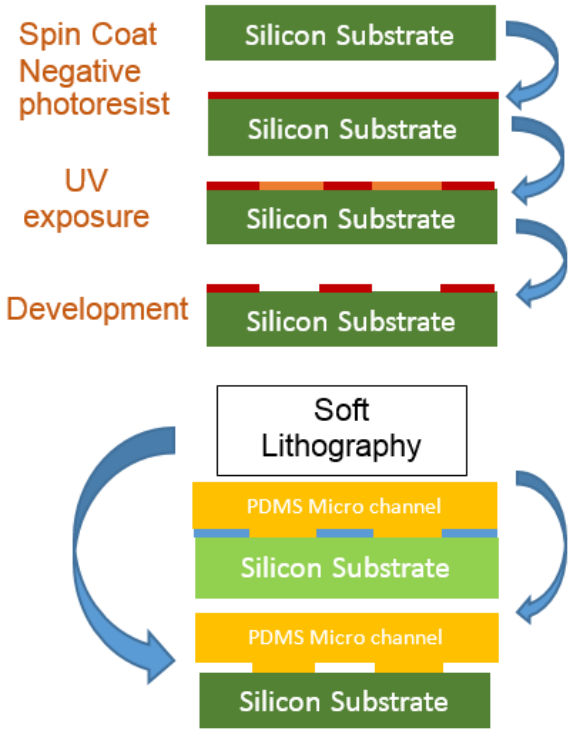

Figure 10: Flow chart of the Photo lithography process used for micro-fabrication process. The second image shows the soft-lithography used to make replicas of the master.

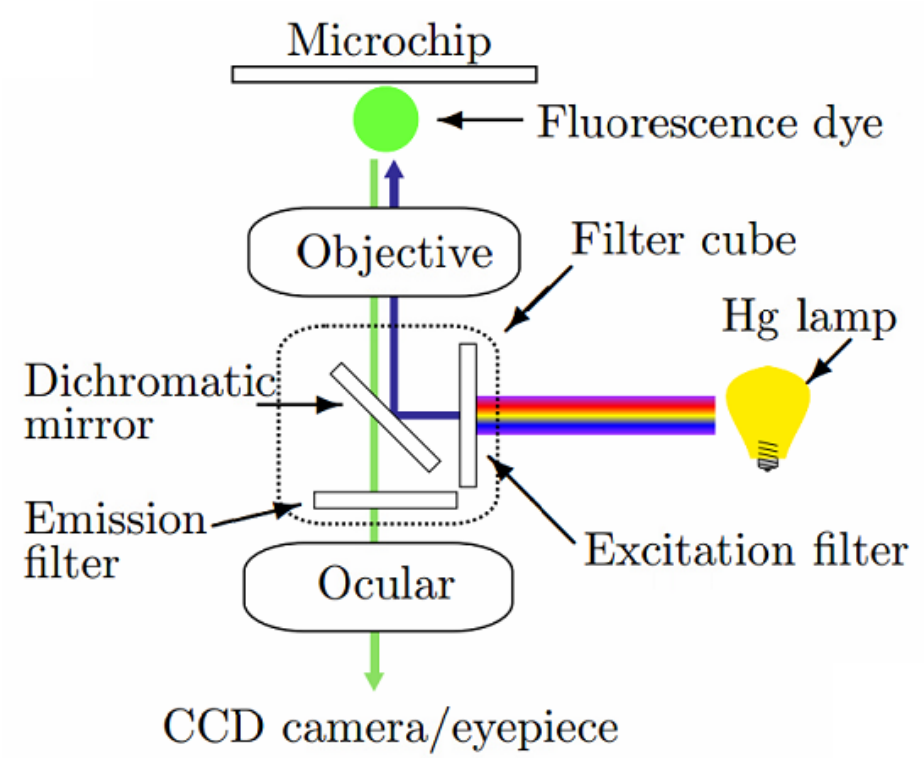

Figure 11: Schematic of the experimental setup, showing the fluorescence microscopy setup.

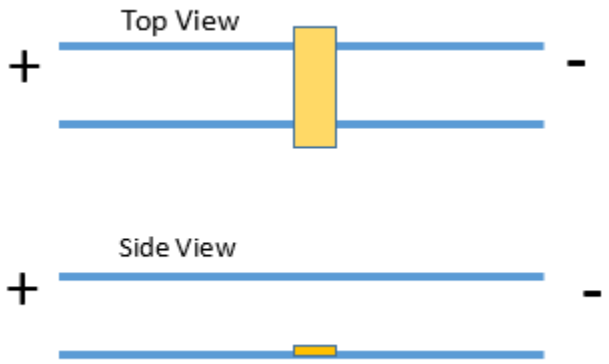

Figure 12: Schematic of the experimental setup. (a) Shows top view of the experiment. (b) Shows the side view. Note that, nafion is present only on the bottom wall. This is clear from (b).

3. Results and Discussion:

The formation of the depletion region is confirmed by the use of fluorescent b-Phycoerythrin dye. When a voltage is applied across the device, an immediate decrease in the fluorescent intensity on the anodic side of the nano-porous membrane is noted. This is due to the depletion of the electrolyte owing to the ion selectivity of the membrane. An overall net electro-osmotic flow towards the cathode is also noted, due to the bulk movement of fluid above the membrane (If the membrane occupied the entire channel cross-section, the bulk movement of fluid due to electro-osmosis is not possible.) In this setup, however, there is no formation of an enrichment region. This is expected as the net bulk electro-osmotic flow will drive any enrichment to the reservoir. Along with the formation of depletion region, field amplified sample stacking and the formation of micro-vortices are observed in the anodic side of the membrane.

3.1 Field Amplified Sample Stacking (FASS)

An increase in the fluorescent intensity of the negatively charged b-phycoerythrin dye adjacent to the depletion region is noted (Figure 14). This increase in fluorescent intensity is however, not the same as ion enrichment as it is not seen adjacent to the membrane. Similar results have been reported by researchers (Bharadwaj and Santiago (2005)), (Ko et al. (2012)) experimenting with electrolyte of different concentrations along the channel. This phenomenon is called field amplified sample stacking or ion pre-concentration and occurs around regions of lower electrolyte concentration.

FASS is explained as suggested by Bharadwaj and Santiago (2005). Field amplified sample stacking occurs due to the changes in conductive gradient resulting in non-uniform electro migration fluxes in an electrolyte. This happens primarily due to changes in the electrolyte

concentration in the system. The Figure 13 shows the working of FASS. Upon application of a potential difference across a sample with conductive gradient, the depletion region acts as a high-electrical-resistance zone in series with the rest of the channel, and electric field is amplified within this region of depletion. In such a condition, the sample ions move from a region of high drift velocity to a region of low drift velocity. This leads to stacking of ions adjacent to the depletion region as shown in Figure 13. Stacking of positively charged ions is absent because any stacking is driven away due to net elecro-osmotic flow. Positively charged Rhodamine G6 dye is used in the experiments and the absence of any pre-concentration of ions is noted, proving the above-mentioned statement. This also explains why the stacking of negatively charged dye molecules increases with time (Figure 14). As more and more analytes are brought to the depletion region due to elecro-osmosis, the negative ions stack up adjacent to it. It is therefore observed that the fluorescent intensity of the negatively charged dye increases with time.

In experiments with nafion, researchers have reported a depletion region with 10-100 times less concentration than the bulk electrolyte. This leads to a large amplification in the electric field in these regions. An important observation in the depletion region is the shape of the stacking front as seen in Figure 13b. Due to the amplification of electric filed in the region, electro-osmotic slip velocity is expected to increase in the depletion region. This local increase in electro-osmotic slip velocity is compensated by a back pressure in the system, to maintain conservation of mass. This explains the parabolic velocity profile due to the induced pressure driven poiseuille flow.

3.2 Generation of Micro-Vortices:

Micro vortices are observed in the depletion region of the device adjacent to the membrane. The direction of vorticity is parallel to the chip substrates. As shown in the Figure 15. Similar results are also observed by Yossifon and Chang (2010). These vortices are observed at all voltage regimes from 5 volts to 50 volts and above. This phenomenon cannot be attributed to electro-osmosis of the second kind near an ion-selective membrane as this theory is only applicable to over-limiting current regime, where the formation of a secondary space charge is applicable. Also, the vortices observed due to electro-osmosis of the second kind are along a plane perpendicular to the ones observed in these experiments. Yossifon and Chang (2010) also report seeing these vortices in the limiting current regimes of ICP, which therefore cannot be electro-osmosis of the second kind. The observed phenomenon cannot be attributed to induced charge electro-osmosis (ICEO) either, as you would expect a pair of vortices across the membrane surface as discussed in section 1.7 (Figure 7). These vortices are formed if the conductive membrane is polarized by a strong electric field and different regions of the membrane surface have different surface charge, resulting in an ejecting flow. Counter rotating vortices, however, are not revealed in the experiments, hence conclude this cannot be ICEO flow.

Further, experiments are performed to understand the physics of this vortex instability noted in the experiments. Firstly, the nafion membrane is suspended (Not attached to the wall) inside the microchannel. This is done by using a pre-cured nafion membrane that is peeled off a glass slide. This membrane piece is then placed inside a micro channel and bonded using an oxygen plasma. These experiments did not show the formation of any vortices.

Side view of the vortex is captured, which reveals the shape of the vortex, as shown in Figure 16. The vortex is seen only adjacent to the membrane, and does not occupy the entire channel

depth. Formation of a secondary and tertiary vortex is also evident form the data captured in the side view. Similar results are reported by other researchers (kim et al.,(2012)) as shown in Figure 18.

3.3 Discussion on the observed vortices:

The shape of the vortex is shown in Figure 16. The non-existence of these vortices in case of suspended membrane, proves that this phenomenon occurs as a direct consequence of non-uniform smoluchowski slip velocity at the walls of the micro-channel in the depletion region. Consider Figure 9a, which shows the ionic concentration as a function of distance near an ion-selective membrane. The ionic concentration at the bottom wall of the depletion region will show such a linear decrease. The electric field is therefore amplified along the bottom wall as shown in Figure 9c, being maximum near the membrane surface where the ionic concentration is the least. This increasing electric field leads to a non-linear smoluchowski slip velocity. Also, in the depletion region, the zeta potential of glass is different from that in the electro-neutral region. The fluid accelerated in this region of increasing electric field. Flow acceleration leads to a back pressure in order to conserve the mass, resulting in a vortex like motion of the fluid. Video recordings from the experiment show the fluid accelerating in this region and therefore leads to the formation of vortices.

When the electric field is first applied, the micro-channel behaves as an open channel, as time progresses, there is a buildup of pressure (i.e. the bulk flow is initially as shown in Figure 2a, and at steady state as shown in Figure 2b). As previously discussed in section 1.2, the open channel velocity profile has a uniform plug like shape. However, in practical microfluidic chips, as the electro-osmotic flow pushes the fluid to one reservoir, there is a backpressure created in the system due to un-equal levels of fluid in the reservoirs. This backpressure builds up over time,

and at steady state, a velocity profile as described in Figure 2b is observed in the upstream and downstream regions. This velocity profile of the bulk fluid leads to the drop-like shape of the vortex. Figure 17shows the shape of the vortex initially (when the system behaves as an open channel), and after the system has reached steady state (pressure builds up to equal the level of liquid in the reservoirs.) Therefore, the amplified electric field causes an increase in the electro-osmotic slip velocity and hence leads to the formation of these vortices. This behavior is seen in all regimes of ohmic, limiting, and overlimiting current.

In summary, the physics of the formation of these vortices is explained as shown in Figure 18. The concentration variation along the bottom wall in the entire channel is shown in Figure 18a. The electrolyte has a bulk concentration far upstream. Closer to the membrane, the electrolyte concentration decreases due to the perm-selective behavior of the membrane and formation of depletion region. Since the membrane with numerous nano-pores can be treated as a 1D model, a linear decrease in the concentration is expected. Further, downstream regions of the channel has a low concentration of electrolyte.

This linear decrease in the concentration leads to an exponential behavior of the electric potential in the depletion region. Figure 18b shows how the electric potential drops along the channel length. In the upstream and far downstream regions of constant electrolyte concentration, a linear drop in the electric potential is expected. The electric field strength can be described as the potential drops per unit distance (i.e. the slope of the cure in Figure 18b). The Electro-osmotic slip velocity is directly dependent on this electric field strength, and therefore behaves as shown in Figure 18c. Since, in this experimental setup, the membrane is patterned on the bottom wall, resulting in the effects of depletion predominantly on the bottom wall. The slip velocity on the bottom wall behaves as shown in Figure 18c. Figure 18d shows this formation of vortex due to an accelerating slip boundary on the bottom wall. The flow at the

wall's upstream and downstream regions has a constant slip velocity. The center of the channel in both upstream and downstream regions has an opposite velocity, due to the pressure induced back flow (closed channel setup). In the depletion region, the fluid accelerates along the bottom wall, which leads to a vortex like motion. This vortex, when seen from a top view, looks like an oscillatory motion of particles.

3.3.1 Multiple Vortices:

Further, the formation of a secondary and tertiary vortex is reported in this experiment (Figure 19). This is similar to the ones seen by Kim et al. (2012). However the vortices seen in these experiments are not counter-rotating, as opposed to the ones seen by Kim et al. (2012). The primary vortex induces the secondary, the secondary induces the tertiary vortex and so on, and all these vortices have the same direction. The flow field around the high speed primary vortex is mostly convection dominated (High Prandtl number). This fast moving primary vortex therefore changes the local concentration in the depletion region. With the negative Y component of the primary vortex leading to local regions of higher concentration adjacent to the primary vortex. This means the concentration dip in the depletion region is not uniform, but has local regions of higher concentration. This leads to the formation of subsequent vortices.

The 1D linear concentration profile discussed in the previous section is the concentration along the bottom wall only. However, since the channel has a finite depth and the electric field lines are affected by the conducting membrane, a concentration profile decreasing linearly along the electric field lines is expected. This leads to a two-dimensionally varying concentration profile, schematically shown in Figure 20, centered at the surface of the membrane. Different concentrations are shown by the different colors in Figure 20, and this 2D variation of concentration occurs primarily due to the electric field lines curving into the conducting

membrane (electric field lines are shown in the background). A fast moving primary vortex, as discussed in the previous section, leads to mixing effects in the device, thereby changing the local concentration. The lower concentration ions near the bottom wall move upwards, and the higher concentration electrolyte move towards the channel wall. This leads to the formation of local regions of higher concentration near the channel wall next to the primary vortex.

A non-linear drop in the electrolyte concentration near the bottom wall occurs due to this mixing effect of the primary vortex (Figure 21a). As a result, the electric potential also changes locally (Figure 21b). Further, this leads to a non-uniform variation of the electric field in the depletion region, thereby leading to a non-uniform acceleration of fluid along the channel walls. The slip velocity along the bottom wall is shown in Figure 21c. This slowing down of fluid in regions of higher concentration leads to the formation of multiple vortices in the system (Figure 21d), each inducing a subsequent vortex of smaller size.

(a)

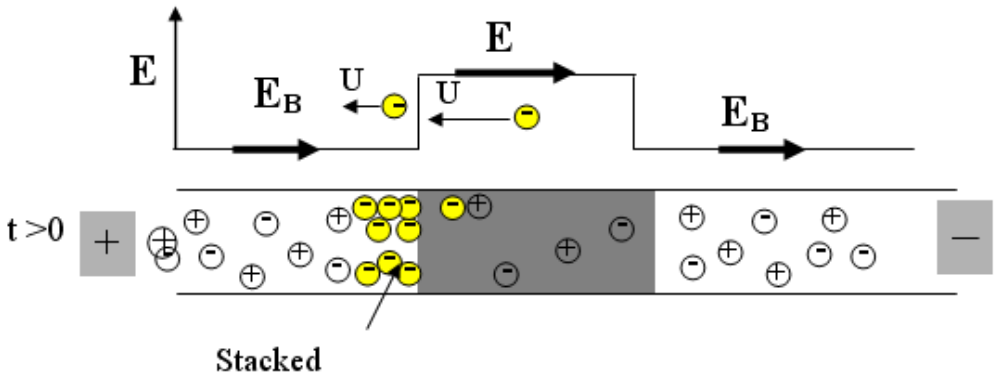

(b)

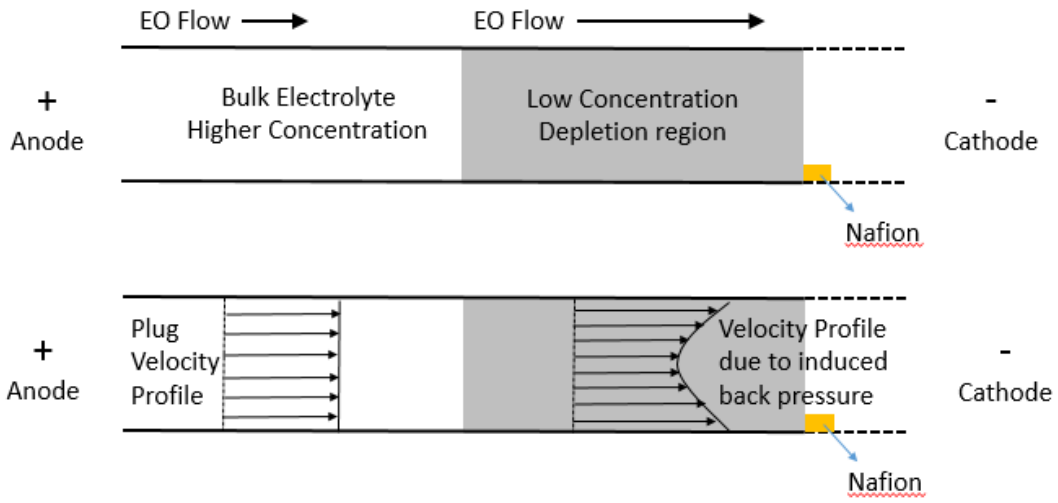

Figure 13: (a) Working of Field Amplified sample stacking (REF). For t>0 after the electric field is applied, it is observed how the negative ions stack at the entrance of the depletion region. (b) Shows the velocity profile in the region of low electrolyte concentration, and bulk

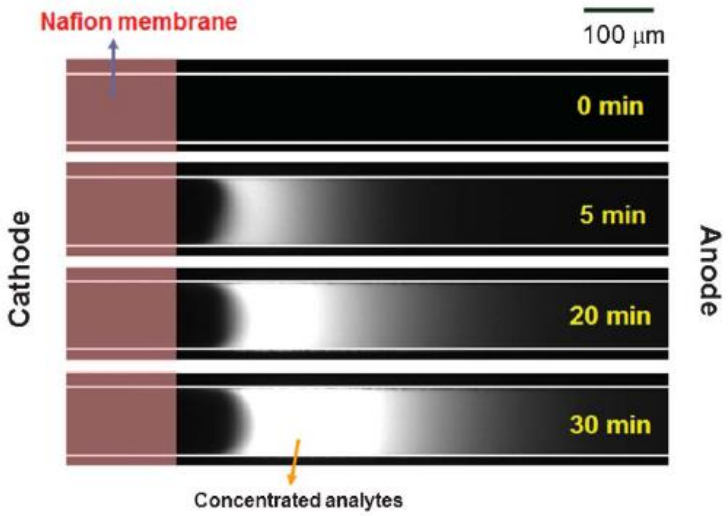

Figure 14: Field Amplified sample stacking. Shows the stacking phenomenon at different times. The shape of the stacking front is also clear. From Kim et al, 2012.

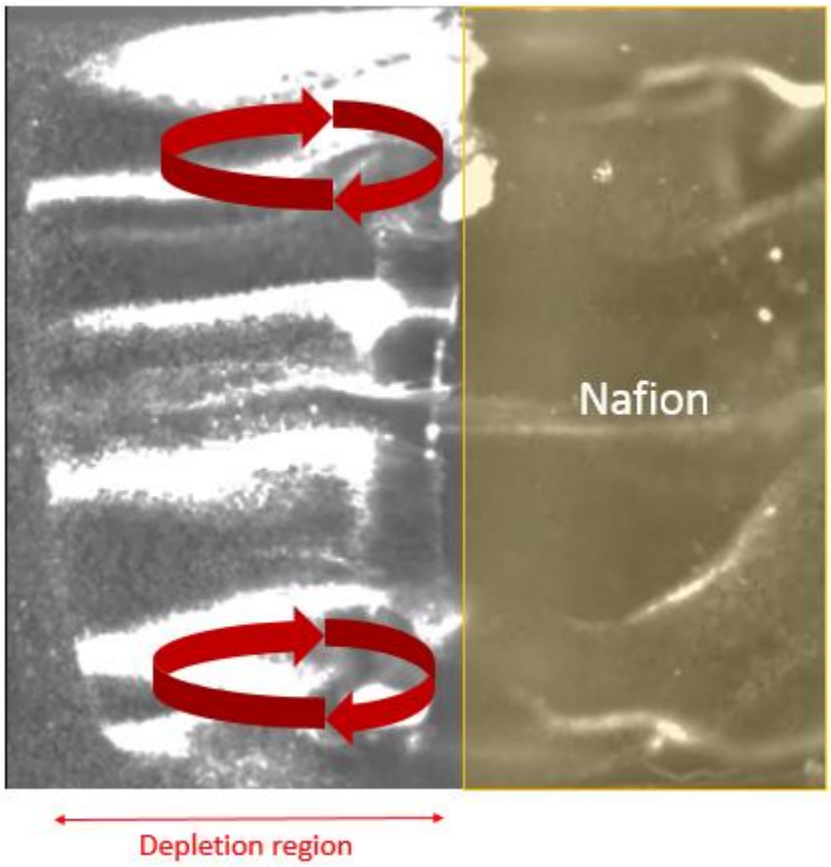

Figure 15: Experimental observation of the vortices formed due to non-uniform slip in the depletion region.

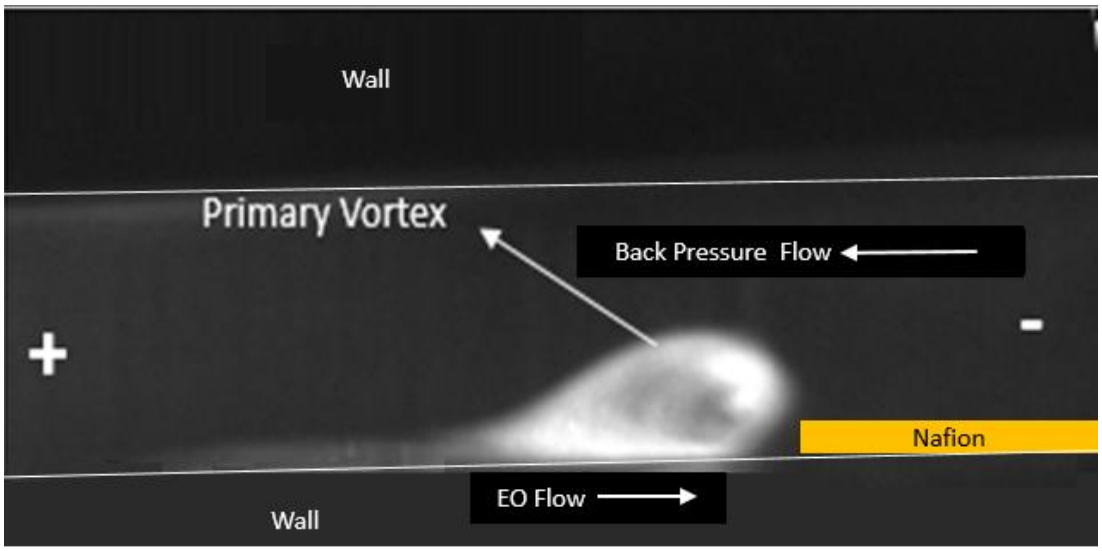

Figure 16: Side view of the vortex in steady state conditions. The tear-drop shape of the vortex is evident. See supplementary video.

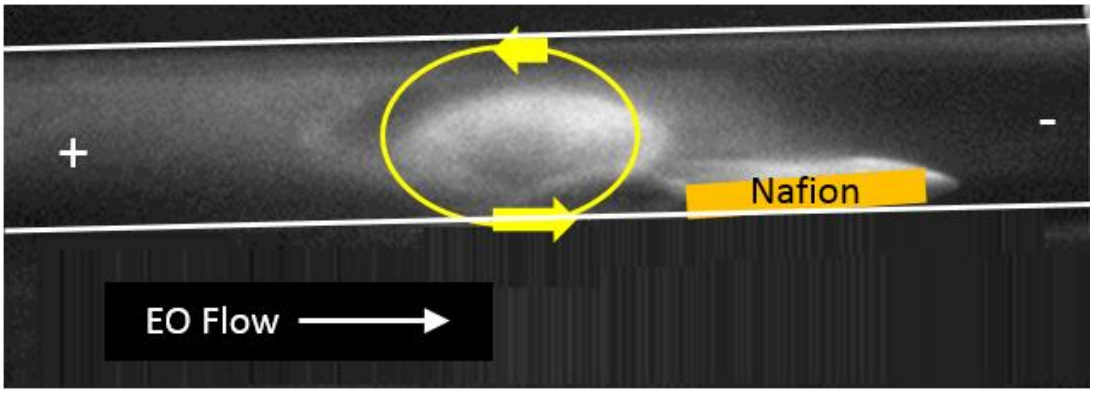

Figure 17: Initial shape of vortex before back pressure builds up in the system.

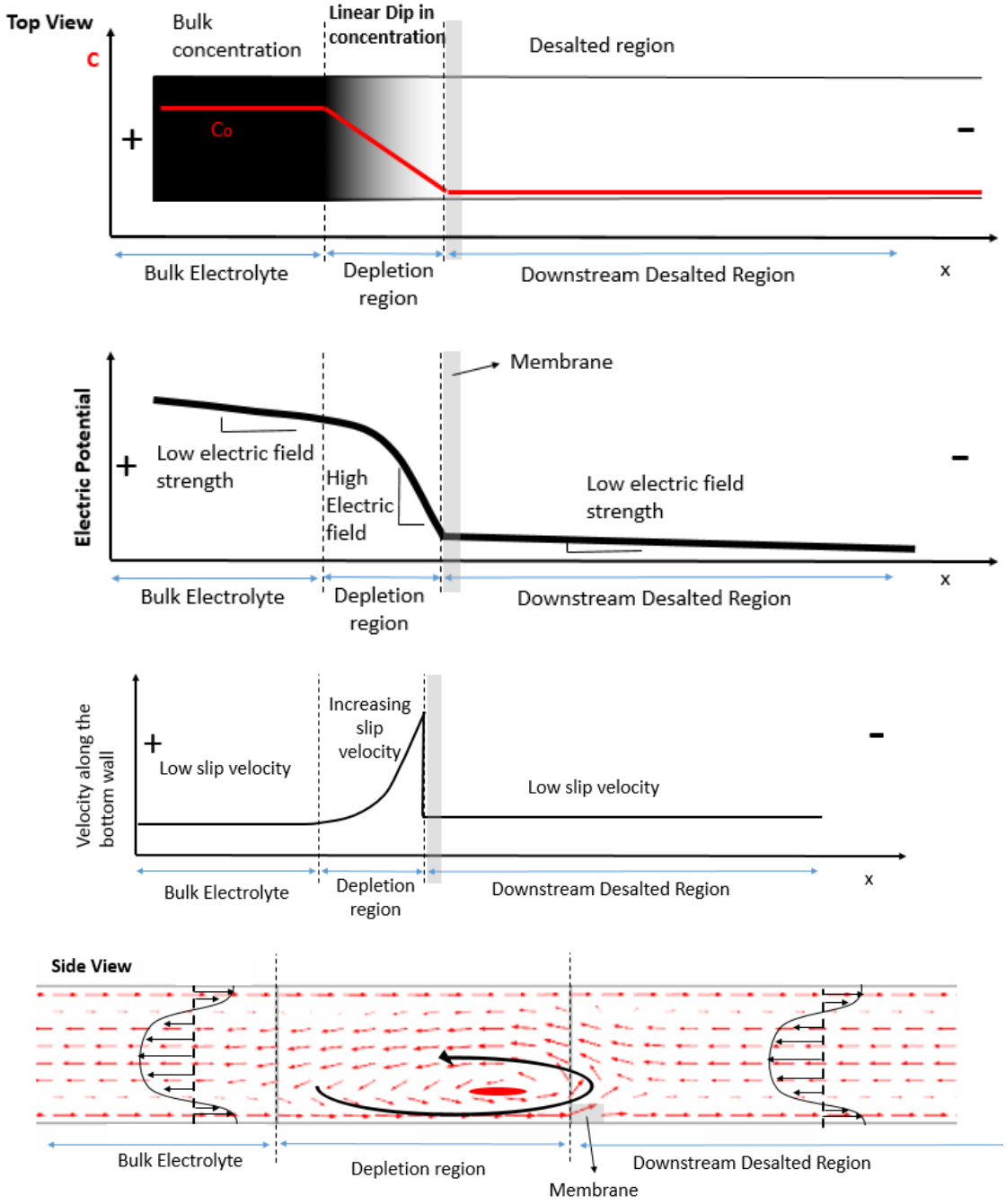

Figure 18: Summarizing the phenomenon of non-linear electro-osmotic slip. (a) Shows the linear dip in concentration. (b) The electric potential along the channel. (c) Electro-osmotic slip velocity and (d) the formation of micro vortices.

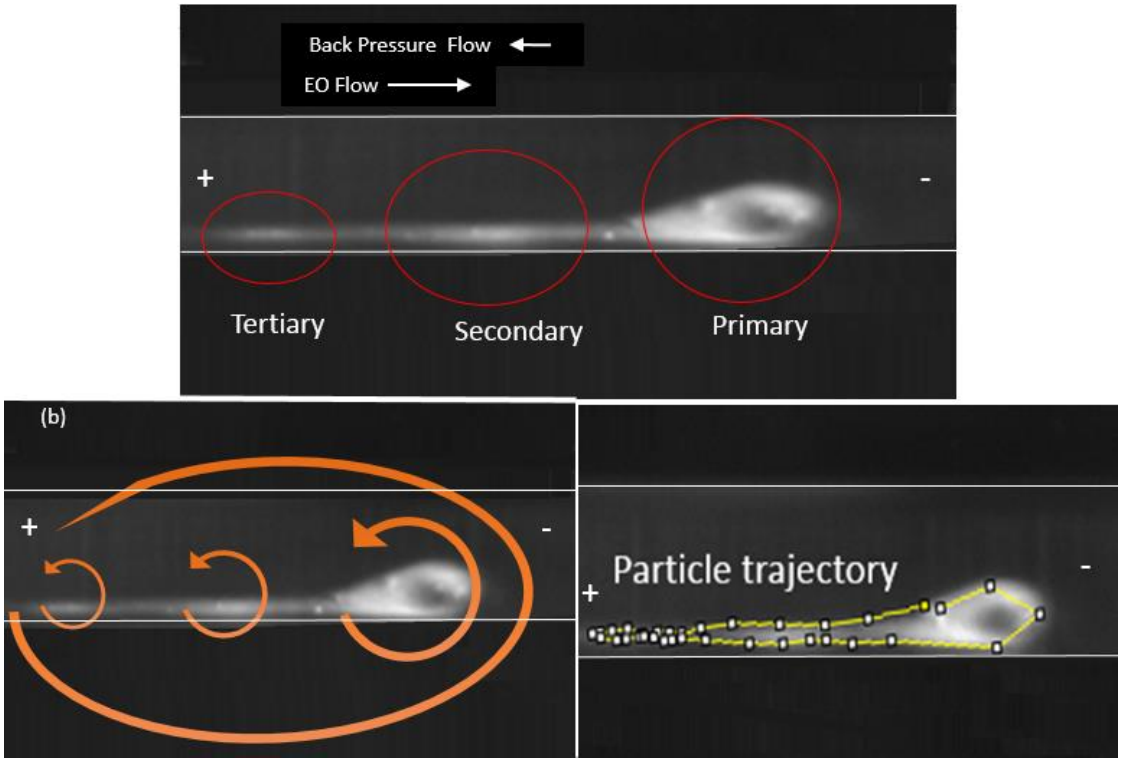

Figure 19: (a) Showing the side view of the three vortices formed in the depletion region. (b) Showing the direction of the three vortices, (c) Trajectory of a single particle that goes around all three vortices.

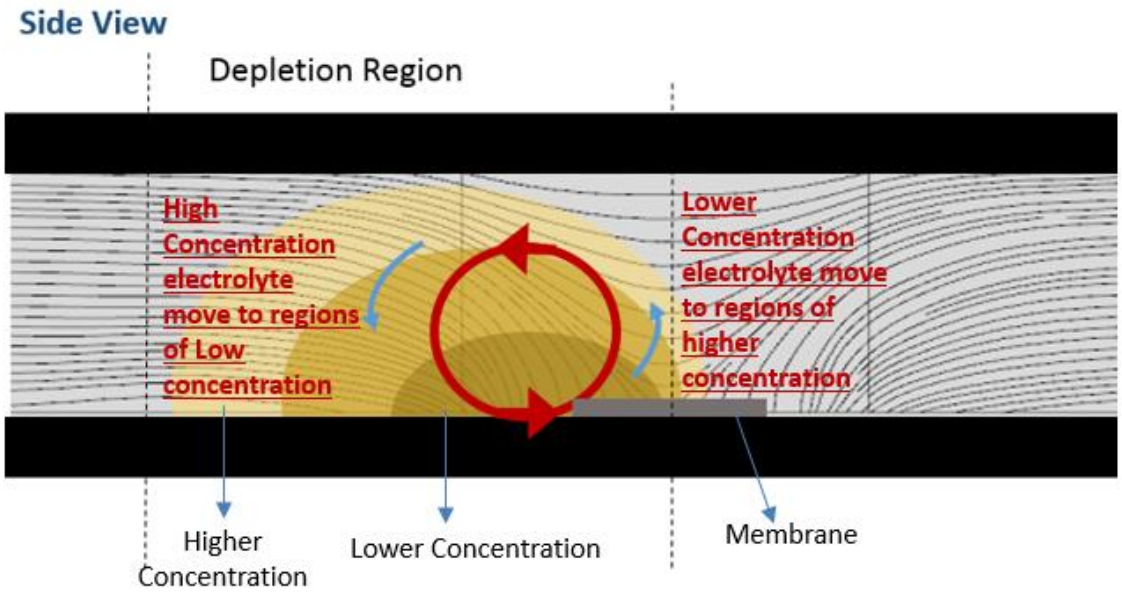

Figure 20: Schematic of the concentration variation in 2D from the side view, and the mixing effect of vortices changing local concentration.

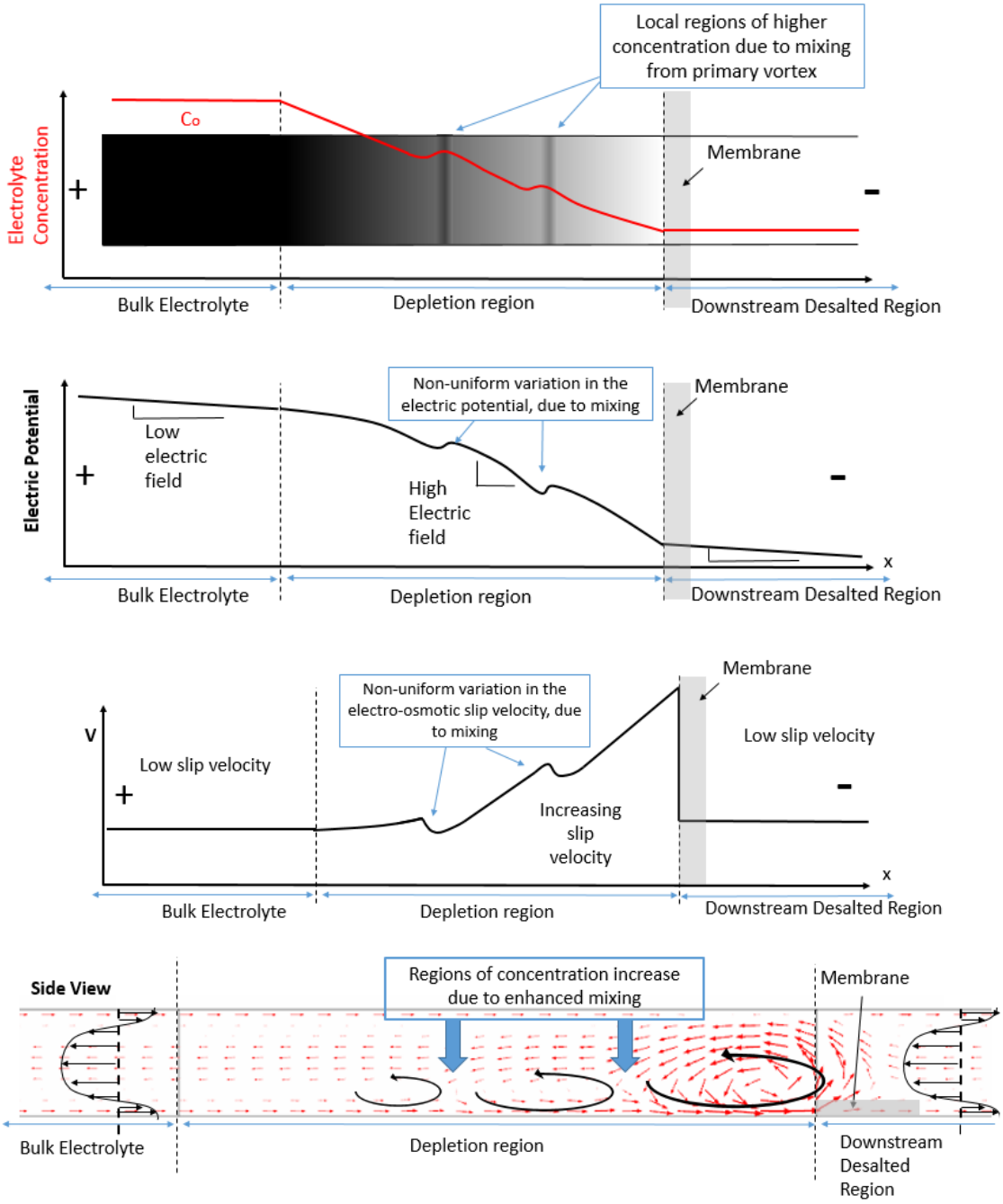

Figure 21: Schematic, showing the formation of multiple vortices. (a) Concentration change in the depletion region near bottom wall. (b)Electric potential in the depletion region. (c) Electro-osmotic slip along the channel's bottom wall. (d) Side view, showing the formation of multiple vortices. Due to enhanced mixing, local region of higher concentration lead to the formation of multiple vortices.

4. Simulation:

2D simulations are performed in COMSOL to understand the hydrodynamic behavior of fluid in the depletion region of the setup. The modelled problem is considered as a simple 2D slipping wall case. The geometry used for simulation consists of a long micro channel 2cm in length and 100 microns in depth. Only the steady state condition is modelled, which means the model behaves as a closed channel setup.

The entire geometry was divided into three regions for, upstream, depletion and downstream regions of flow. COMSOL uses a finite element method to solve the partial differential equations, which requires the geometry to be divided into a subdomains called elements. The three regions are divided into elements using an unstructured triangular mesh.

The equations for the model are implemented by manipulating the built-in physics equations of the software. The following form of steady state Navier-Stokes equation is solved for in-compressible flow.

$$\rho(\nabla.\bar{\mathrm{u}}) = 0$$

$$\rho(\bar{\mathrm{u}}.\nabla)\bar{\mathrm{u}} = \nabla.[-\mathrm{pI} + \mu(\nabla\bar{\mathrm{u}} + (\nabla\bar{u})^{T})] + F$$

Here, I is the identity matrix, superscript T stands for matrix transpose.

Boundary conditions are applied on the walls of the model (Figure 22). A stationary wall boundary condition is imposed on the inlet and outlet lines (1 and 5). This ensures the closed channel behavior of the model, leading to a back pressure driven flow. A slipping boundary condition with a slip velocity scaling to smoluchowski slip velocity on all the walls, except in the depletion region (2, 3, 4, 5 and 7). An interpolation function is used to apply an accelerating slip boundary condition on the wall in depletion region (wall 6). The interpolation function used scales according to the ones predicted in Figure 9. In this experimental setup, the cured nafion is

1-2 um, which is small compared to the size of the channel (100um). The height of the nafion membrane can be therefore assumed to be negligible and not modelled.

Results from the simulation show the formation of a vortex in the accelerated flow region. It is evident that the closed channel behavior of the system leads to the tear drop shape of the vortex (Figure 23a,b). This is similar to the experimental measurements from the side view of the channel. The vortex extends throughout the depletion region, and the length of the vortex increases as the size of the depletion region enlarges.

Further, experiments also reveal the formation of a secondary and tertiary vortex that are adjacent to the primary vortex (Section 3.3.1). As discussed previously, these subsequent vortices are in the same direction, and are induced by the primary vortex. The mixing effect leads to local areas of flow deceleration along the channel's bottom wall. To model this non-uniform acceleration, bumps are added to the slipping wall boundary condition.

This non-uniform boundary condition along the bottom wall reveals the formation of multiple vortices in the depletion region. Figure 24 shows the results from simulating a flow with localized region of deceleration due to localized decrease in the electric field. These results show the formation of multiple vortices in the same direction.

These simulations are only solving the hydrodynamics, and intended to reveal the nature of flow only. They do not tell us much about the size, and the effects of mixing in the channel. They, however, are a good for predicting the nature vortices in the flow.

4.1 Vortex Identification:

Since numerical analysis performed is that of a steady state one, the streamlines reveal the existence of vortices in the flow. However, to confirm the existence of vortices, methods suggested by Jeong and Hussain (1995) are used. Results from the delta method are as shown in

Figure 25a. Regions of vortex formation are colored, and this figure reveals the existence of three vortices.

These results, however, are different from the ones reported by Kim et al. (2012). Multiple vortices in the same direction as the primary vortex are reported in this thesis. Kim et al. (2012) report the existence of counter rotating vortices due to a step decrease in the concentration profile. Similar hydrodynamic simulations are performed to analyze this model with a step decrease in concentration as suggested by these researchers. A step increase in slip velocity, however, does not reveal the formation of multiple vortices (Figure 25b). Instead, only a single vortex is seen, and no counter rotating multiple vortices are observed.

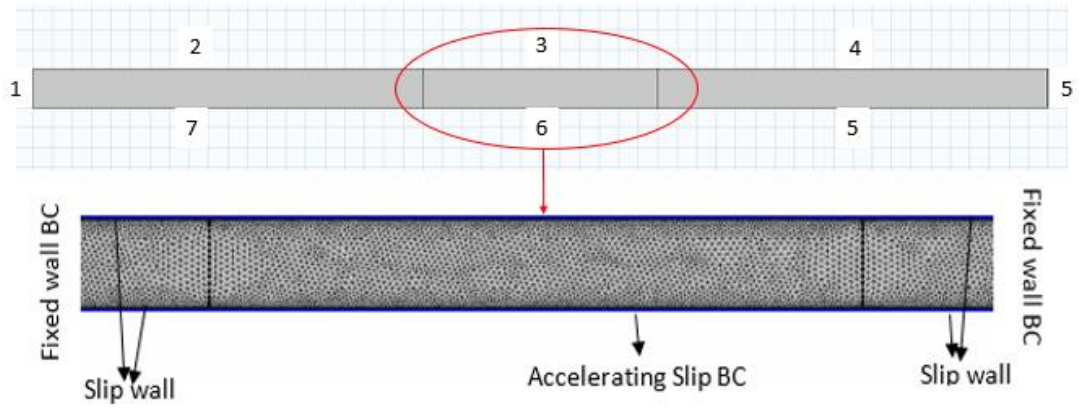

Figure 22: Geometry used for the numerical analysis, along with the applied boundary conditions. Mesh used for the simulation is also shown in the second figure.

(a)

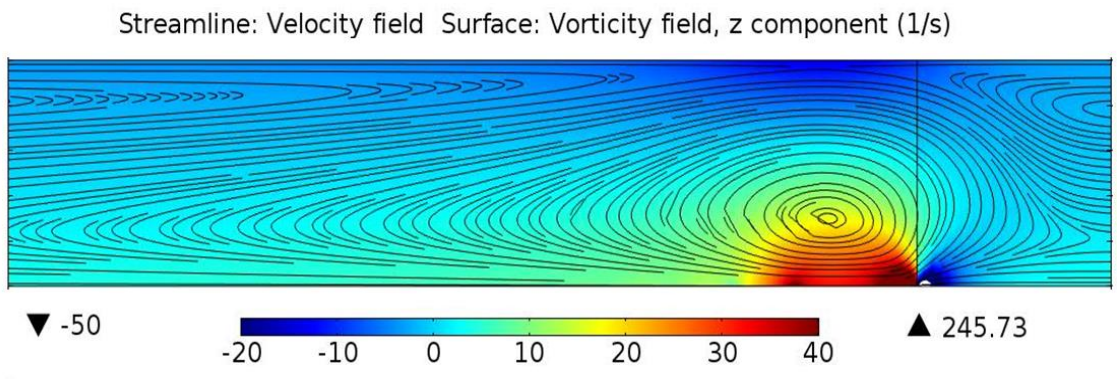

(b)

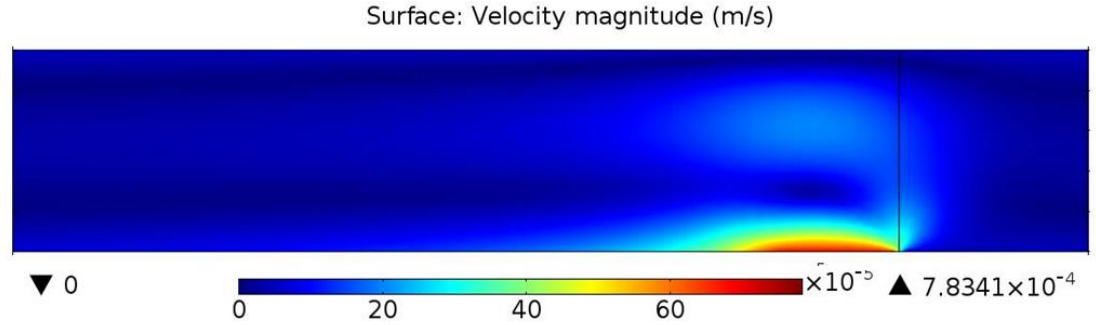

Figure 23: (a) Stream lines and vorticity from non-uniform acceleration boundary condition. (b) Velocity magnitude

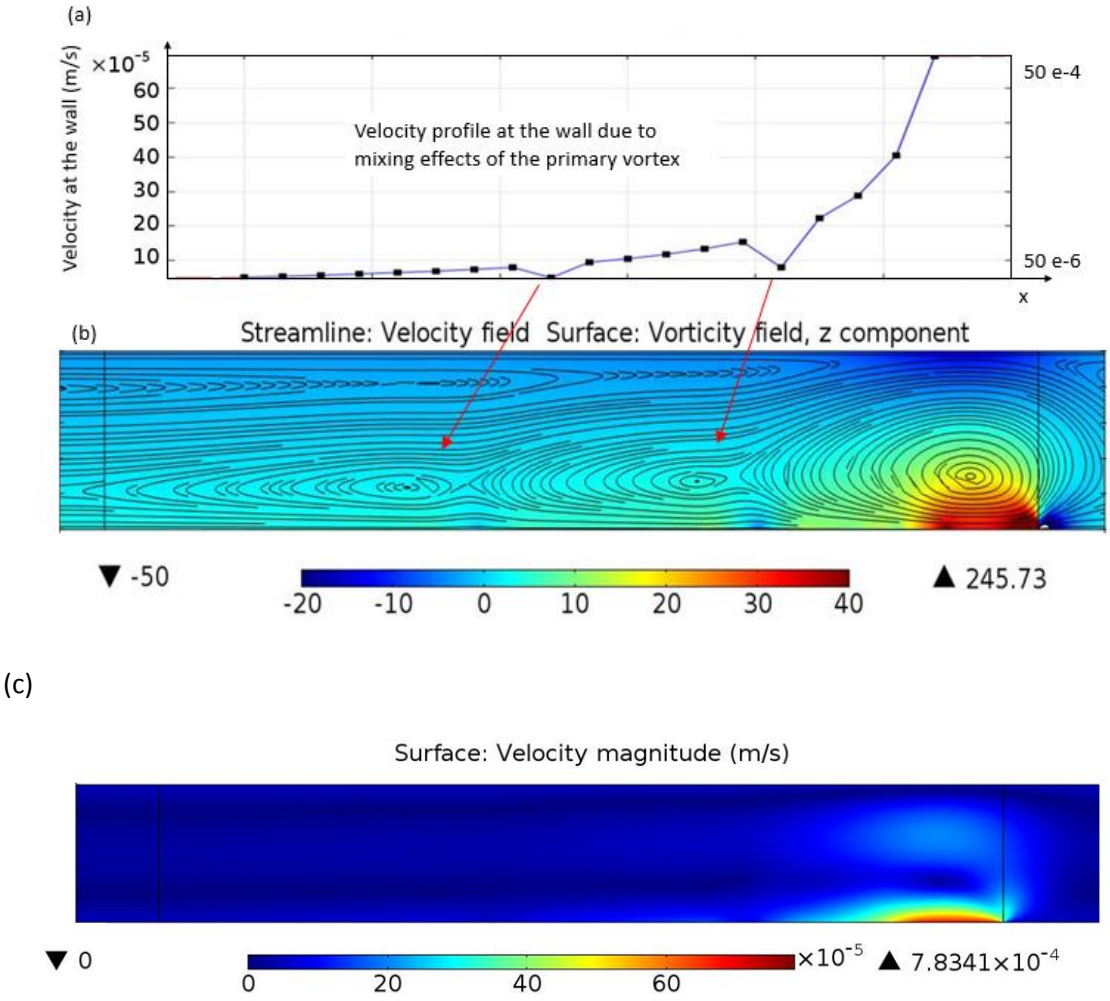

Figure 24: Shows the results from simulation, the effect of mixing and formation of secondary, and tertiary vortex. (a) Slip velocity at the wall. (b) Streamlines and vorticity (c) Velocity magnitude in the channel.

(a)

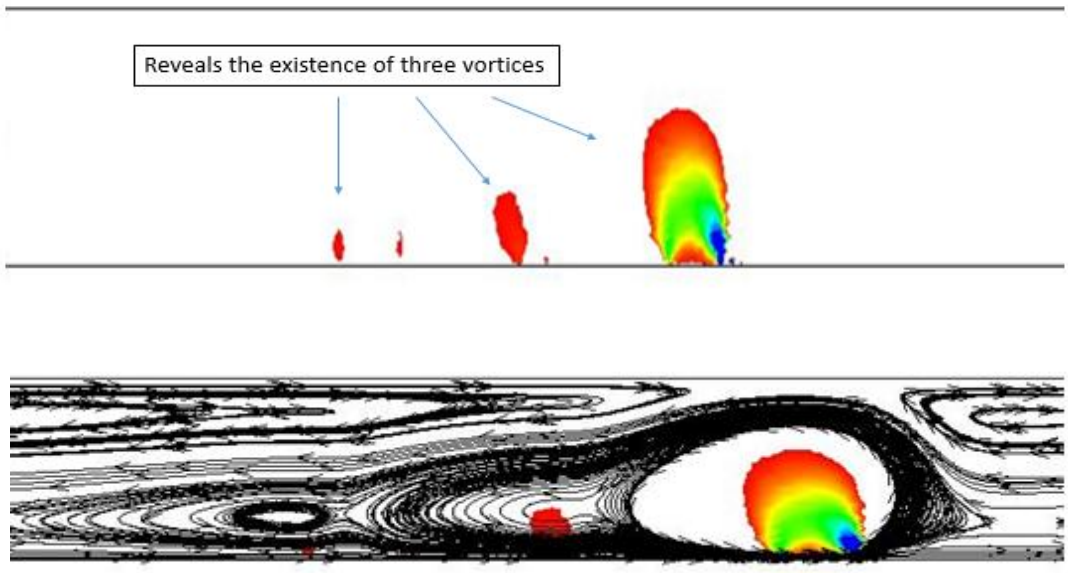

(b)

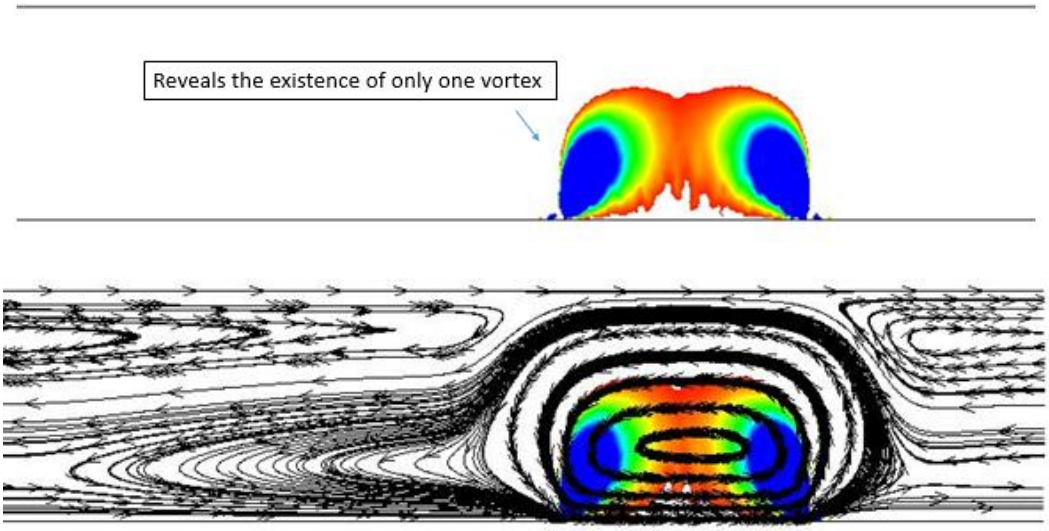

Figure 25: Detection of vortex by delta method. (a) Highlights the regions where the vortex exists, overlap of streamlines for the velocity profile assumed in model described in section 3.3.1. (b) Overlap of streamlines and predictions by delta method for the velocity profile as predicted by kim et al, 2012.

5. Conclusion:

An experimental study on single channel electrokinetic pre-concentrator, which incorporates a nano-porous membrane inside a micro-channel, is presented. Researchers, for pre-concentration and other purposes have previously used this setup. The aim is in reviewing the concepts of field amplified sample stacking and formation of vortices in the depletion region adjacent to the nano-porous membrane. The results in the experiments conducted on pre-concentration are similar to the ones obtained in the literature, and are successful in demonstrating the working of a simple pre-concentration device.

Fluorescent particles are used to track the flow and observed the formation of high speed vortices adjacent to the nano-porous membrane. Explaining the formation is the primary motive of this study, and experiments and simulations are conducted to understand the same. It captures the side video the vortex, and the tear drop shape can be observed. Multiple vortices adjacent to the primary vortex, all having the same direction are reported.

In the depletion region an amplification of the electric field, leads to an increased smoluchowski slip velocity. This increase in slip velocity leads to a rotating vortex flow adjacent to the nano-porous membrane. Particles moving in both directions in the channel far from the membrane, showing the velocity profile of combined electro-osmotic flow and pressure driven flow are observed.

The results obtained, are backed by basic numerical simulation of an accelerating wall in a micro channel. These results also reveal the formation of multiple vortices which are induced by the primary vortex. The mixing effect of the primary vortex leads to a non-linear decrease in the electrolyte concentration in the depletion region, leading to local regions of higher concentration. This in turn affects the slip velocity and leads to the formation of multiple vortices.

Further, this analysis can be useful in controlling the formation, size and shape of these vortices. Which could lead to better fluid handling, manipulation, separation and mixing techniques in micro-fluidic systems.

References:

Bazant, M., & Squires, T. (2004). Induced-Charge Electrokinetic Phenomena: Theory and Microfluidic Applications. *Physical Review Letters*, *92*(6).

Bharadwaj, R., & Santiago, J. G. (2005). Dynamics of field-amplified sample stacking. *Journal of Fluid Mechanics*, *543*(-1), 57.

Chang, H.-C., & Yeo, L. Y. (2010). *Electrokinetically driven microfluidics and nanofluidics*. Cambridge; New York: Cambridge University Press.

Duknin, S. S. (1991) Electrokinetics of second kind. Advances in colloidal and interface science. 35 (173-196).

Jeong, J., & Hussain, F. (1995). On the identification of a vortex. *Journal of Fluid Mechanics*, *285*, 69–94.

Kim, S. J., Ko, S. H., Kwak, R., Posner, J. D., Kang, K. H., & Han, J. (2012). Multi-vortical flow inducing electrokinetic instability in ion concentration polarization layer. *Nanoscale*, *4*(23), 7406.

Kim, S. J., Li, L. D., & Han, J. (2009). Amplified Electrokinetic Response by Concentration Polarization near Nanofluidic Channel. *Langmuir*, *25*(13), 7759–7765.

Kim, S., Wang, Y.-C., Lee, J., Jang, H., & Han, J. (2007). Concentration Polarization and Nonlinear Electrokinetic Flow near a Nanofluidic Channel. *Physical Review Letters*, *99*(4).

Ko, S. H., Song, Y.-A., Kim, S. J., Kim, M., Han, J., & Kang, K. H. (2012). Nanofluidic preconcentration device in a straight microchannel using ion concentration polarization. *Lab on a Chip*, *12*(21), 4472.

Lee, J. H., Song, Y.-A., & Han, J. (2008a). Multiplexed proteomic sample preconcentration device using surface-patterned ion-selective membrane. *Lab on a Chip*, *8*(4), 596.

Lee, J. H., Song, Y.-A., & Han, J. (2008b). Multiplexed proteomic sample preconcentration device using surface-patterned ion-selective membrane. *Lab on a Chip*, *8*(4), 596.

Li, D. (2004). *Electrokinetics in Microfluidics*. Academic Press.

Lin, H., Storey, B. D., Oddy, M. H., Chen, C.-H., & Santiago, J. G. (2004). Instability of electrokinetic microchannel flows with conductivity gradients. *Physics of Fluids*, *16*(6), 1922.

Masliyah, J. H., & Bhattacharjee, S. (2006). *Electrokinetic and Colloid Transport Phenomena*. John Wiley & Sons.

Rubinstein, I., & Zaltzman, B. (2000). Electro-osmotically induced convection at a permselective membrane. *Physical Review E*, *62*(2), 2238.

Rubinstein, I., & Zaltzman, B. (2010a). Dynamics of extended space charge in concentration polarization. *Physical Review E*, *81*(6).

Rubinstein, I., & Zaltzman, B. (2010b). Extended space charge in concentration polarization. *Advances in Colloid and Interface Science*, *159*(2), 117–129.

Rubinstein, S., Manukyan, G., Staicu, A., Rubinstein, I., Zaltzman, B., Lammertink, R., … Wessling, M. (2008). Direct Observation of a Nonequilibrium Electro-Osmotic Instability. *Physical Review Letters*, *101*(23).

Squires, T. M., & Bazant, M. Z. (2004). Induced-charge electro-osmosis. *Journal of Fluid Mechanics*, *509*, 217–252.

Thamida, S. K., & Chang, H.-C. (2002). Nonlinear electrokinetic ejection and entrainment due to polarization at nearly insulated wedges. *Physics of Fluids*, *14*(12), 4315.

Wang, S., Yu, H., Wang, W., & Li, Z. (2012). Nanofluidic device with self-assembled nafion membrane utilizing capillary valve. In *Nano/Micro Engineered and Molecular Systems (NEMS), 2012 7th IEEE International Conference on* (pp. 657–660).

Yossifon, G., Mushenheim, P., & Chang, H.-C. (2010). Controlling nanoslot overlimiting current with the depth of a connecting microchamber. *EPL (Europhysics Letters)*, *90*(6), 64004.

Yossifon, Gilad, & Chang, H.-C. (2010). Changing nanoslot ion flux with a dynamic nanocolloid ion-selective filter: Secondary overlimiting currents due to nanocolloid-nanoslot interaction. *Physical Review E*, *81*(6).

Yossifon, Gilad, Mushenheim, P., Chang, Y.-C., & Chang, H.-C. (2009). Nonlinear current-voltage characteristics of nanochannels. *Physical Review E*, *79*(4).

Yossifon, Gilad, Mushenheim, P., Chang, Y.-C., & Chang, H.-C. (2010a). Eliminating the limiting-current phenomenon by geometric field focusing into nanopores and nanoslots. *Physical Review E*, *81*(4).

Yossifon, Gilad, Mushenheim, P., Chang, Y.-C., & Chang, H.-C. (2010b). Eliminating the limiting-current phenomenon by geometric field focusing into nanopores and nanoslots. *Physical Review E*, *81*(4).

Zaltzman, B., & Rubinstein, I. (2007). Electro-osmotic slip and electroconvective instability. *Journal of Fluid Mechanics*, *579*, 173.

Zhao, C., & Yang, C. (2012). Advances in electrokinetics and their applications in micro/nano fluidics. *Microfluidics and Nanofluidics*, *13*(2), 179–203.